ADVANCED MATERIALS

The Effect of an Active Substrate on Nanoparticle-Enhanced Fluorescence**

By *Shy-Hauh Guo, Shu-Ju Tsai, Hung-Chih Kan, De-Hao Tsai, Michael R. Zachariah,* and *Raymond J. Phaneuf**

Strong resonant coupling between light and plasmons in noble metal particles of nanometer dimensions leads to a number of striking and technologically important optical effects, among them surface enhanced Raman scattering (SERS)[1] and the enhancement of fluorescence from nearby molecules.[2] While each of these show great promise for the development of highly sensitive biochip detectors,[3,4] fluorescence is the technique of choice for many biological assays. Significant enhancement here would greatly enhance the sensitivity of these assays to a host of target biomolecules. To date, the maximum enhancement available in fluorescence has not been established. This is largely due both to difficulties in controlling the size and shape of the particles, and to the multiplicity of contributing factors: increased radiative decay rate and enhanced electric fields at resonance, ''hot spots'', i.e. regions of high field between closely spaced particles. The substrate is known to play a role as well; in particular there have been suggestions that certain substrates might play an active role in light-plasmon coupling rather than merely shifting the resonance frequency, as would a conventional glass substrate. Here we report observations of just such an effect, in which the size dependence of the enhancement of fluorescence from monodisperse silver nanoparticles is profoundly altered by the use of a Si substrate. Comparing fluorescence measurements with calculations of the response of the silver nanoparticles to incident light, we show that unlike what is commonly assumed, the variation of the fluorescence enhancement with nanoparticle diameter does not simply follow that of plasmon excitation as measured by the optical extinction. Instead we find that it is the generation of regions of high electrical field intensity near the particle which dominates the fluorescence enhancement we observe, and that the silicon substrate plays an active role in this regard: sweeping these regions out from beneath the particles as their size approaches the optimum for fluorescence.

1. Results

In Figure 1 we compare scanning electron microscopy images and fluorescence microscopy images from size-selected, fluorescently-tagged silver nanoparticles on a silicon substrate over a range of particle diameters. In Figure 1(a)–(e) the SEM images are shown in red, and fluorescence images for an excitation wavelength of 514 nm (exciting the Cy3 fluorophore), scanned from precisely the same regions are superposed in green. The SEM images show that particles are spherical, and randomly distributed. There are rare occasions where two or more particles are in contact; this occurs more frequently on samples with larger average particle diameter, as shown in Figure 1(e). In general, however, individual particles are well separated from their neighbors. The fluorescence intensity shows a strong and systematic variation from image to image, i.e. as the average diameter of the Ag nanoparticles is varied. Highest intensities are obtained from samples with particle diameters slightly below the middle of the range we have studied, i.e. for $d \approx 90$ nm. A similar trend, but with a slight increase in the optimum diameter is also observed from fluorescent images for an excitation wavelength of 633 nm, as discussed below.

Individual fluorescence images show considerable variation of the intensity from point to point within an image. This is apparently due to variation in the coverage of the tagged protein. We base this on the following observations: (1) we find that spatial variation of the intensity remains fixed when additional images of the same region are scanned, (2) many of the bright regions occur between relatively well separated Ag nanoparticles, and (3) there are no extremely intense ''hot spots'' between particles in near – contact[5] or in agglomeration. Interestingly, however there is a correlation between fluorescence and local coverage for certain particle

[*] Prof. R. J. Phaneuf
     Department of Materials Science and Engineering
     University of Maryland, College Park, MD 20740, (USA)
     E-mail: phaneuf@lps.umd.edu
     S.-H. Guo
     Department of Electrical and Computer Engineering
     University of Maryland, College Park, MD 20740, (USA)

     S.-J. Tsai, D.-H. Tsai
     Department of Materials Science and Engineering
     University of Maryland, College Park, MD 20740, (USA)

     H.-C. Kan
     Department of Physics
     University of Maryland, College Park, MD 20740, (USA)

     Prof. M. R. Zachariah
     Department of Mechanical Engineering and Department of Chemistry
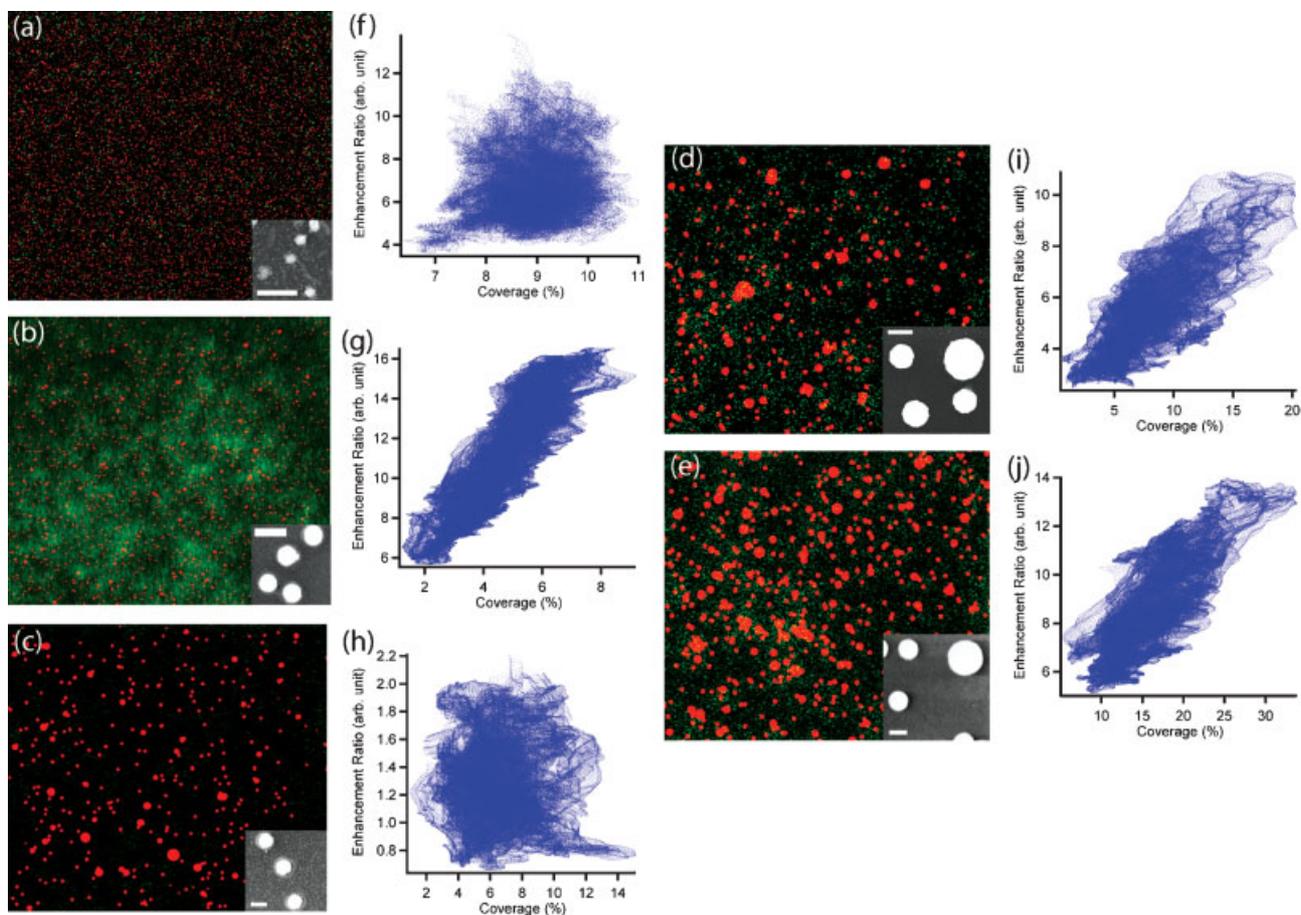   University of Maryland, College Park, MD 20740, (USA)

Figure 1. (a)–(e) SEM images (red) of the Ag nanoparticles deposited on silicon substrates, and the corresponding fluorescent images (green) for Cy3 fluorophore scanned with LSM from the same cell: The field of view is 20 μm. (f)–(j) Fluorescent intensity vs. local Ag nanoparticle coverage determined from panels (a)–(e), using 2.5 μm bins. The average particle diameters in each panel are (a), (f) 67 ± 1 nm, (b), (g) 96 ± 2 nm, (c), (h) 173 ± 24 nm, (d), (i) 271 ± 14 nm, and (e), (j) 319 ± 17 nm. The inset in panels (a)–(e) show higher magnification SEM images allowing the particle shapes to be seen; the size of the scale bar in the insets is 200 nm.

sizes, those for which the image-averaged intensity is a maximum. In Figure 1(g) the overall enhancement is a maximum, and local intensity varies linearly with local Ag nanoparticle coverage; a somewhat less good linear correlation is seen Figure 1(i) and 1(j). The observed linear dependence suggests that the variations in intensity from image to image should be associated with effects due to individual particles. Images for nanoparticles producing little enhancement in the fluorescence show intensity and coverage that are essentially uncorrelated, as seen in Figure 1(f) and 1(h).

Quantitative analysis of the fluorescence enhancement for Cy3 and Cy5 fluorophores from the silver nanoparticles is shown in Figure 2(a) and 2(b), respectively. We define the coverage corrected enhancement $N = \frac{I_a - I_B}{I_f - I_B}$, with $I_a = \frac{I_e - (1 - A_a) \cdot I_f}{A_a}$, where I_a is the average fluorescent intensity corrected for the area fraction of the surface covered by the silver nanoparticles,[6] A_a (which in turn is determined by SEM image analysis). I_e is the local raw fluorescence intensity measured from the area covered with fluorophore/spacer coated silver nanoparticles, I_f is the fluorescent intensity

measured from an area covered with a fluorophore/spacer layer, but no silver nanoparticles, I_B is the "background" intensity, measured from an area where neither fluorophore nor silver nanoparticles are present. An important issue in this analysis is whether the fluorescently tagged proteins cover both the Ag nanoparticles and the substrate. We resolve this unambiguously by measuring atomic force microscopy (AFM) force curves from Ag nanoparticles and the substrate before and after depositing the fluorescently-tagged protein. We find that the adhesive force, measured on withdrawing the tip while under a buffer solution is large and different without protein deposition: 21 nN from the Ag nanoparticles vs. 10 nN from the surrounding substrate. The adhesive force is nearly identical and much smaller, ~1 nN, after deposition. We conclude that both the nanoparticles and substrate are coated with protein. Figure 2 shows the measured nanoparticle diameter dependence. As shown in panel 2(a), the enhancement initially increases with particle diameter, reaching a maximum of approximately 240 at $d \approx 85$ nm for the 514 nm wavelength excitation; we observe a window of particle diameters between
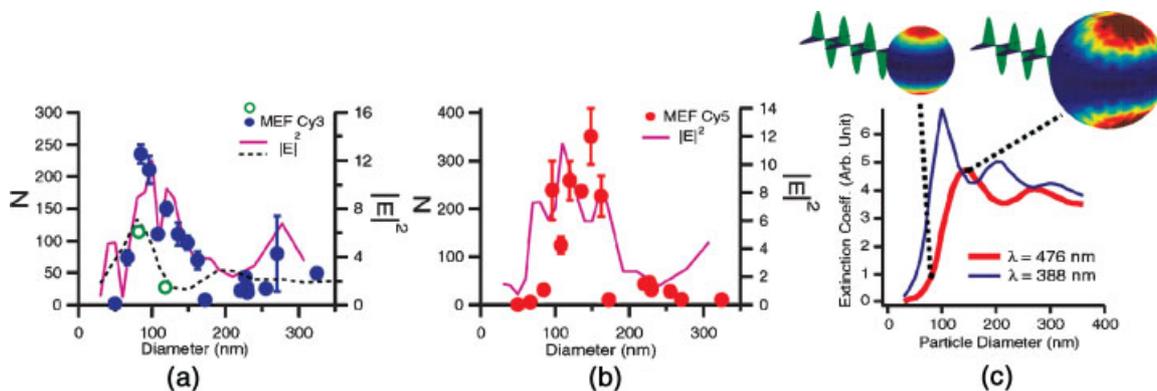
Figure 2. Measured normalized enhancement of the fluorescence, N, on silicon substrate (filled circles) or glass substrate (open circles), and the calculated average E-field intensity (solid curve) near the Ag particles as a function of Ag particle diameter: (a) 514 nm excitation (Cy3 fluorophore), (b) 633 nm excitation (Cy5 fluorophore). The dashed curve in (a) shows the same averaged E-field intensity calculated for the case of glass substrate. (c) Calculated extinction coefficient and electrical field intensity, E^2, (with $|E|$ normalized to incident amplitude) for silver nanoparticles. Extinction coefficients are plotted as a function of particle diameter for incident light wave length fixed at 476 nm (633 nm in air) in red curve and 388 nm (514 nm in air) in blue curve. Insets show the E^2 distribution over a spherical surface 8 nm from the surface of silver particles with diameter of 80 nm and 150 nm, respectively. The incident light represented by the sinusoidal modulations is traveling toward the particle, and the E-field is polarized in the vertical direction (colored in green). The color scale indicates the field intensity normalized to that of the incident light.

$\approx$85 nm and $\approx$150 nm for which the enhancement exceeds 100 fold. For excitation at a wavelength of 633 nm, the maximum enhancement of approximately 350 is measured at a slightly larger diameter, $\approx$150 nm, as seen in panel 2(b); the enhancement exceeds 100 for diameters from $\approx$95 nm to $\approx$160 nm. Much lower or no enhancement is obtained for particle sizes outside these "high-enhancement windows".

To understand the origins of the fluorescence enhancement dependence on particle size, we calculate the response of silver nanoparticles to incident light, using the discrete dipole approximation.[7,8] In our experiment, the silver nanoparticles are always immersed in a thin layer of dilute buffer solution. Thus we assign the index of refraction of the space outside of the silver particle to that of water[9] for all calculations. For simplicity, in our calculations we model the incident light as a linearly polarized plane wave. Our SEM images show that the average particle separation well exceeds the individual diameters; therefore we limit our numerical calculations to the case of a single silver nanoparticle. We begin with the simplest geometry, i.e. freely standing spherical silver nanoparticles. Figure 2(c) shows the calculated extinction coefficients, normalized to the geometric cross section of the particle as a function of particle diameter. The thin blue curve is for an excitation wavelength of 388 nm in water, corresponding to 514 nm in air. The thick curve is for excitation at 476 nm in water, or 633 nm in air. These two curves display qualitatively similar trends: the extinction coefficient first increases with particle diameter reaching a maximum, (at ca. 100 nm for the former case and $\approx$140 nm for the latter case) then oscillates around a slow decaying tail. Significantly, this behavior is qualitatively inconsistent with the abrupt drop in enhancement beyond the high-enhancement windows shown in Figure 2(a) and 2(b). Adding the substrate to the calculation might be expected to change the trend quantitatively, but not qualita-

tively.[10] This difference in behavior contrasts with a simple identification of fluorescence enhancement with resonant coupling between the incident light and plasmons in the silver nanoparticles. A hint as to the origin of this discrepancy comes from the calculated distribution of electrical field intensity[11] near the particle shown in the insets. We note that the fluorescence intensity is expected to be proportional to the local intensity $\left|\vec{E}\right|^2$. The leftmost inset shows the spatial variation of the calculated E-field intensity, normalized to that of the incident light in the vicinity of an 80nm diameter silver particle, for a wavelength of 476 nm. While the optical extinction from silver nanoparticles in this size range is small, there is nonetheless a strong E-field enhancement in regions near the top and the bottom poles of the particle. The rightmost inset shows that as the particle diameter increases to 150 nm, close to where the maximum optical extinction occurs, the regions of high E-field shift away from poles of the particle. Significantly, the main effect of the particle size is in the spatial distribution, rather than the maximum value of the field strength.

We now consider how the silicon substrate affects this picture. Simple models of the enhancement based entirely upon the plasmon resonance suggest it should simply red-shift the resonance. We include it in our calculation, treating it as a finite square slab of silicon[12] placed behind the particle in the direction of the wave vector $\vec{k}$ of the incident light. The lateral dimension of the silicon slab is chosen as three times the diameter of the silver particle; larger sizes are precluded by computer memory and practical computing time. We vary the thickness of the silicon slab from 75 nm to 450 nm, but find that this does not change the qualitative trend of the result. Figure 3 shows how the calculated E-field distribution in the azimuth of incident E-field polarization changes with the size of the silver nanoparticles; here a 150 nm thick silicon substrate and an
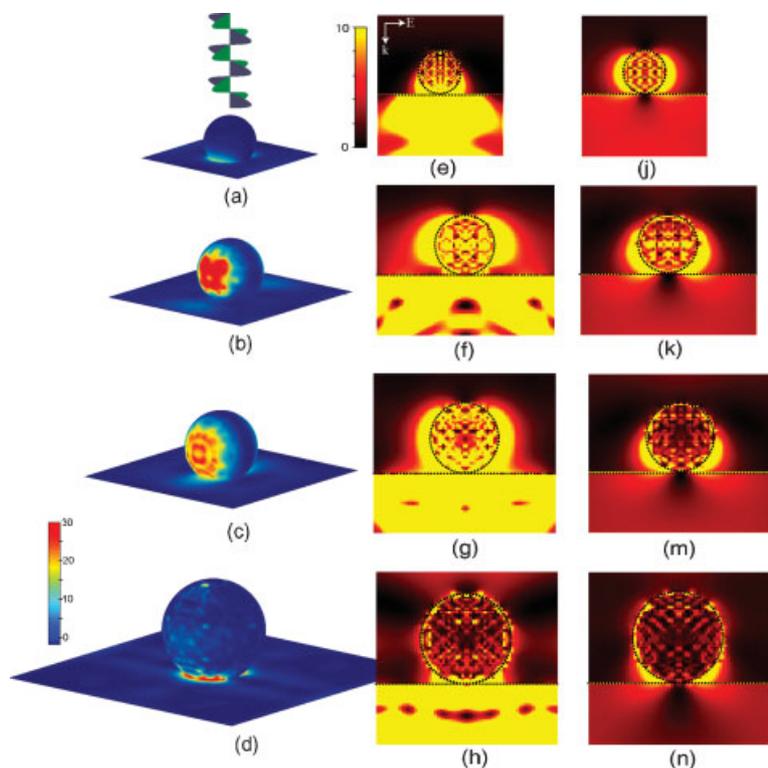
Figure 3. Calculated electric field intensity (E^2) distribution at the distance 8 nm from the surface of the silver nanoparticle and the silicon substrate. The particle diameters are 60, 100, 120, and 210 nm for panels (a), (b), (c), and (d), respectively. As shown in panel (a), the incident light propagates downward and the polarization of the E-field is parallel to the substrate (colored in green). The wavelength of the incident light is 388 nm wavelength (514 nm in air). The color table indicates the field intensity normalized to the incident light intensity. Panels (e), (f), (g) and (h) are cross sectional renderings of electric field intensity (E^2) for particle diameters of 60, 100, 120, and 210nm, respectively; panels (j), (k), (m) and (n) are cross sectional renderings of the electric field intensity (E^2) for the same particle diameters, but on a SiO$_2$ substrate.

incident light wavelength of 388 nm in water (514 nm in air) are used. Figure 3(a) and 3(e) are 3D and cross-sectional renderings, respectively, of the calculated intensity $\left|\vec{E}\right|^2$ for a relatively small diameter of 60 nm. As can be seen most clearly in the cross-sectional view, the silicon substrate, because of its large dielectric function, has a profound effect on the field; for this size the strongest field enhancement occurs beneath the particle. As shown in Figure 3(b) and 3(f), increasing the particle size to 100 nm, close to the observed optimum in Figure 2(a), causes regions of strong E-field enhancement to sweep upward, to the regions at and above the equator of the particle. A further slight increase in particle diameter to 120 nm results both in a slight downward sweep of the high field regions (Fig. 3(c) and 3(g)), and a decrease in the measured enhancement (Fig. 2(a)). Increasing the particle size further, to 210 nm, both sweeps the regions of high E-field back into the region beneath the particle as shown in Figure 3(d) and 3(h), and causes a dramatic drop in the measured intensity (Fig. 2(a)).

This sweeping of regions of high field, and its correlation to the observed fluorescence enhancement demonstrate the

profound effect of coupling to the silicon substrate. Both the particles and substrate are opaque at these wavelengths; only the fluorescent emission from molecules located in regions which are not shadowed by the particles can be observed. Remarkably, *this active substrate has a strong effect on the size-dependence of fluorescence enhancement in the presence of a substrate.* As a rough means of accounting for the shadowing effect in our calculation, we average the E-field intensity, i.e. $\left|\vec{E}\right|^2$, over only that region of the particle for which no shadowing occurs. Based upon the known thickness of the protein and spacer layer, the fluorescent tags are between 4–12 nm from the surface of the silver nanoparticles. We thus calculate the E-field intensity averaged over a hemi-spherical surface 8 nm from the particle surface opposite the substrate. We note that although regions of high field also exist within the substrate, no fluorescent molecules exist there. Summary plots of the size dependence of this averaged E-field intensity for the two excitations are shown as solid curves in Figure 2(a) and 2(b). Good agreement between the measured fluorescence enhancement and the calculation is evident in both cases. This result shows that the distribution of the enhanced E-field intensity is crucial to the measured fluorescence enhancement, and leads to an important insight: *as the particle size varies, regions of electrical field enhancement shift position; maximum fluorescence enhancement occurs when a large fraction of those fluorophores which are not shadowed by either the particles or substrate are immersed in regions of high field; low or no enhancement occurs otherwise.*

Our results thus demonstrate that coupling to an active substrate plays a striking, and unexpected role in the optimum enhancement of fluorescence by metal nanoparticles. Fluorescence from molecules located in close proximity to silver nanoparticles on a silicon substrate depends strongly on the particle diameter, with optimum enhancement of at least 350 fold; the silicon substrate controls the regions of strong electric field, and in particular for which particle diameters are these regions not shadowed by the particles themselves. This effect is even more striking when compared to the field intensity which results from a more conventional, passive substrate, SiO$_2$. Figure 3(j)–(n) show the calculated $\left|\vec{E}\right|^2$ distribution for the same particle sizes as for the Si substrate. The substrate perturbs the field much less strongly, resulting in a conventional dipole-like distribution for smaller particles, and mixed dipolar/quadrupolar distribution at larger diameters. The resulting $\left|\vec{E}\right|^2$ versus size dependence is shown as the dashed curve in Figure 2(a). The maximum is shifted to a smaller diameter, and reduced by approximately a factor of 2; measurements of the fluorescence enhancement for a SiO$_2$ substrate, shown by the open circles in Figure 2(a) indeed show approximately half of the

enhancement measured using a Si substrate. The effect we see is similar to the hot-spot effect between particles which is believed to be responsible for the observation of single molecule sensitivity in SERS.[4] Here, however it is the "hot regions" around single particles, where high electrical field and thus large enhancement occurs. We thus find that it is essential to include the spatial distribution of the field near the nanoparticles into consideration for optimizing design of biosensors employing plasmonic response from metallic nanoparticles. We expect this new insight to lead to advances in the development of highly sensitive biochips. We further note that the work presented here represents only a limited optimization; we anticipate that the use of other active substrates, possibly with the introduction of a spacer layer for tunability, will produce even larger enhancements.

Experimental

We synthesize spherical silver nanoparticles by spray pyrolysis,[13] charge them and then pass them through a differential mobility analyzer (DMA)[14,15] for size-selection; next we sinter them in hydrogen to make them spherical. We deposit these spherical, size-selected particles onto a Si(001) substrate [14,16] which we pre-pattern with a square grid of crossed lines using photo-lithography; this allows navigation to the same position with both scanning electron microscopy (SEM) for particle metrology and laser scanning microscopy (LSM) for fluorescent imaging. We obtain statistics of the size and the number density of the particles by analyzing the SEM images scanned from the sample.[17] All of the measurements reported here are done in regions away from the grid lines, i.e. on the bare Si substrate. We vary the average diameter of the nanoparticles over the range from 50 nm to 320 nm, and find a maximum of 7% standard deviation from the average. The areal coverage of the particles varies from 4% to 15% between samples; we correct for this variation, as described below. We coat the nanoparticle-covered substrates with a BSA-biotin spacer layer, whose thickness is 3–4 nm. Next we deposit drops of solution containing both Cy3 and Cy5 fluorophore-tagged complementary streptavidin protein. Finally we rinse away fluorophore-tagged protein which is not bound to underlying BSA-biotin. Fluorescent images of the sample are collected using a confocal laser scanning microscopy (Zeiss model LSM 410). The samples are maintained wet, i.e., under a thin layer of dilute buffer solution (pH 7.5, 5mM solution of mixture of NaH_2PO_4 and $Na_2HPO_4 \cdot 7H_2O$). For the Cy3 fluorophore the wavelength of the incident (excitation) light is 514 nm, produced by an Argon laser, and the fluorescent image is collected through a filter which passes wavelengths between 535 nm and 575 nm wavelength. For the Cy5 fluorophore the wavelength of incident light is 633 nm, produced by a He-Ne laser, and the fluorescent image is collected through a filter which passes 660 nm wavelength and above.

[1] M. Moskovits, *Rev. Mod. Phys.* **1985**, *57*, 783.

[2] J. R. Lakowicz, *Anal. Biochem.* **2001**, *298*, 1.

[3] a) J. Zhao, X. Zhang, C. R. Yonzon, A. J. Haes, R. P. V. Duane, *Nanomedicine* **2006**, *1*, 219. b) L. R. Hirsh, J. B. Jackson, A. Lee, N. J. Halas, J. L. West, *Analyt. Chem.* **2003**, *75*, 2377. c) S. W. Bishnoi, C. J. Rozell, C. S. Levin, M. K. Gheith, B. R. Johnson, D. H. Johnson, N. J. Halas, *Nanolett.* **2006**, *6*, 1687.

[4] S. Nie, S. R. Emory, *Science* **1997**, *275*, 1102.

[5] E. Hao, G. Schatz, *J. Chem. Phys.* **2004**, *120*, 357.

[6] T. D. Corrigan, S.-H. Guo, H. Szmacinski, R. J. Phaneuf, *Appl. Phys. Lett.* **2006**, *88*, 101112.

[7] B. T. Draine, P. J. Flatau, *J. Opt. Soc. Am. A* **2004**, *11*, 1491.

[8] P. B. Johnson, R. W. Christy, *Phys. Rev. B* **1972**, *6*, 4370.

[9] G. M. Hale, M. R. Querry, *Appl. Opt.* **1973**, *12*, 555.

[10] a) T. R. Jensen, M. L. Duval, K. L. Kelly, A. A. Lazarides, G. C. Schatz, R. P. V. Duyne, *J. Phys. Chem. B* **1999**, *103*, 9846. b) M. D. Malinsky, K. L. Kelly, G. C. Schatz, R. P. V. Duyne, *J. Phys. Chem. B* **2001**, *105*, 2343.

[11] We have developed a Fortran program to calculate the E-field distribution based on the dipole moments using the discrete dipole approximation method.

[12] G. E. Jellison, Jr., *Opt. Mater.* **1992**, *1*, 41.

[13] T. C. Pluym, Q. H. Powell, A. S. Gurav, T. L. Ward, T. T. Kodas, L. M. Wang, H. D. Glicksman, *J. Aerosol Sci.* **1993**, *24*, 383.

[14] D.-H. Tsai, S. H. Kim, T. D. Corrigan, R. J. Phaneuf, M. R. Zachariah, *Nanotechnology* **2005**, *16*, 1856.

[15] a) H. J. Fissan, C. Helsper, H. J. Thielen, *J. Aerosol Sci.* **1983**, *14*, 354. b) S. H. Kim, M. R. Zachariah, *Nanotechnology* **2005**, *16*, 2149.

[16] D.-R. Chen, D. Y. H. Pui, *J. Nanoparticle Res.* **1999**, *1*, 115.

[17] E. Rencs, S.-H. Guo, unpublished.